INSTITUTE OF PHYSICS PUBLISHING JOURNAL OF PHYSICS B: ATOMIC, MOLECULAR AND OPTICAL PHYSICS

J. Phys. B: At. Mol. Opt. Phys. **34** (2001) 1727–1744 www.iop.org/Journals/jb PII: S0953-4075(01)17121-X

Electron-impact single ionization of krypton ions (q = 12–18)

M Khouilid[1], S Cherkani-Hassani[2], S Rachafi[1], H Teng[3] and P Defrance[2]

[1] Université Chouaäb Doukkali, Faculté des Sciences, km1, Route Ben Maachou, BP 20, El Jadida, Morocco
[2] Université Catholique de Louvain, Département de Physique, Chemin du Cyclotron 2, B-1348 Louvain-la-Neuve, Belgium
[3] Institut für Kernphysik, Justus-Liebig-Universität Giessen, D-35392 Giessen, Germany

Received 14 September 2000, in final form 18 January 2001

Abstract

Absolute cross sections for electron-impact single ionization of krypton ions Kr^{q+} (q = 12–18) have been measured. The animated crossed-beam method has been applied. The measurements cover the energy range from threshold to about 5.5 keV. The presence of ions formed in metastable states is observed for Kr^{18+}, Kr^{16+} and Kr^{14+}. Inner-shell excitation from the 2s, 2p, 3s and 3p subshells followed by autoionization is seen to play a dominant role for this reaction over the whole energy range. The importance of these excitation–autoionization processes explains the large underestimation of cross sections from the available theoretical and semi-empirical estimations which include direct processes only.

1. Introduction

For the design of future thermonuclear reactors, krypton has been recognized as a good candidate for spectroscopic diagnostics of, for instance, the temperature at the plasma edge, as well as in the central plasma where the electron temperature may be of the order of 20–40 keV. For this reason, a good knowledge of related spectroscopic and collisional atomic data is needed in order to interpret the observation of various plasma parameters (Janev 1993). Among the processes playing a role in this field, electron-impact ionization of atoms and ions is a fundamental one, because it governs the ion charge state distribution evolution in the plasma. Consequently, the corresponding ionization cross sections are required for plasma modelling.

The status of the knowledge of the electron-impact ionization process has been analysed in detail (Defrance *et al* 1995) for ions of thermonuclear interest. For single ionization (SI), there have been few reports of absolute electron-impact ionization cross sections for multicharged krypton ions (Defrance 1995). Experimental cross sections for Kr^{q+} (q = 1–11) have been published: for example, for charge states 1 (Man *et al* 1987, Tinschert *et al* 1987), 2 (Man *et al* 1993, Tinschert *et al* 1987, Gregory 1985), 3 (Gregory *et al* 1983, Tinschert *et al* 1987), 4, 5 and 7 (Bannister *et al* 1994), 8 (Bannister *et al* 1988), 9 (Gregory and Bannister 1994) and 10 and 11 (Oualim *et al* 1995). Theoretical cross sections have been obtained for charge states 4–7

(Gorczyca *et al* 1994a), 10–11 (Teng *et al* 2000) and 18 (Younger 1982). Energy thresholds corresponding to ionization and excitation of outer- or inner-shell electron are estimated from the Hartree–Fock structure calculation of Blanke *et al* (1992).

In this paper, the first absolute cross section measurements are reported for electron-impact single ionization of multicharged krypton ions Kr^q ($q = 12$–18). These results cover an energy range from below threshold to about 5.5 keV. The presence of ions formed in metastable states is carefully investigated. The respective roles of direct and indirect processes are analysed in detail. In order to explain the results for Kr^{18+}, a calculation is performed in the average configuration distorted-wave (ACDW) approximation in the case where the ion is formed in the first metastable excited state.

2. Method and apparatus

In this experiment, the animated crossed-beams method (Defrance *et al* 1981) has been employed. The present apparatus is described in detail elsewhere (Duponchelle *et al* 1995). It has been specially designed to study electron-impact single and multiple ionization of multiply charged ions (X^{q+}) up to $q = 20$ in an electron energy range from 20 to 6000 eV.

The device is shown schematically in figure 1. The krypton ion beam is extracted from an electron cyclotron resonance (ECR) ion source (1), designed to produce ions from gas or metals by using the sputtering method (Barué *et al* 1998). Ion beams are accelerated by a voltage of 10 kV, mass-analysed (2), focused and deflected to the collision region by a vertical lens (3) and by two cylindrical deflectors (4), (5). The beam is collimated to a cross section of 2×4 mm^2 before crossing the electron beam (6). The magnetic mass analyser (7) separates the product ions $X^{(q+m)+}$ from the primary ions X^{q+}. The product ions are transmitted via a spherical deflector (10) to the channeltron detector (11) while the primary ions are collected

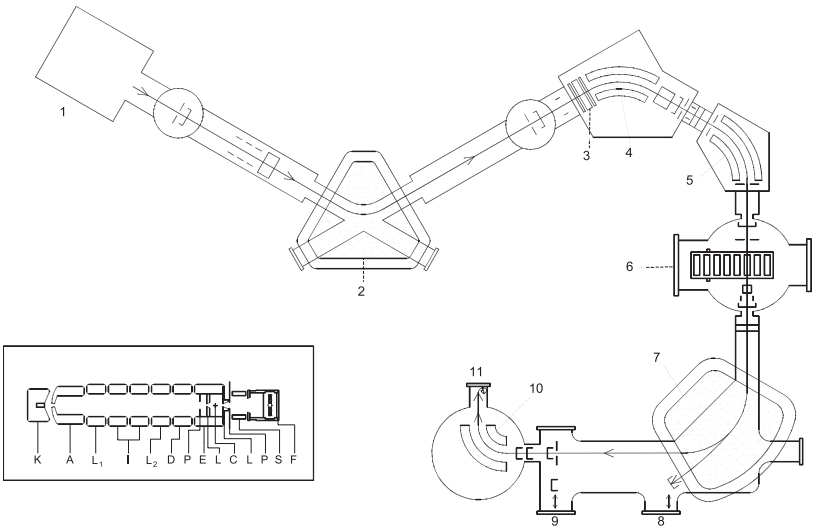

Figure 1. Schematic representation of the apparatus: 1, ECR ion source; 2, magnetic mass selector; 3, electrostatic lens; 4, 5, cylindrical deflectors; 6, collision chamber; 7, magnetic analyser; 8–9, Faraday cups; 10, spherical detector; 11, channeltron detector. The inset shows a schematic plan of the electron gun: K, cathode; A, anode; L1–L2–I, focusing electrodes; D, deflectors; P-S, suppressors; E, final electrodes; L, slits; C, collision region; F, Faraday cup.

by a Faraday cup (8) or (9), depending on the initial and final ion charges. The high-voltage electron gun is shown schematically in the inset in figure 1. The ribbon electron beam is produced in a Pierce cathode–anode configuration by an indirectly heated cathode (K). The anode (A) forms a pair of parallel plates, which is used as the first element of a pair of two electrostatic plane asymmetric lenses. These are designed to progressively accelerate the electrons to their final energy. The pairs of electrodes (L1) and (L2) are the central parts of the first and of the second lens, respectively. They are separated by the intermediate electrode (I). Electrodes (D) act as a beam deflector and plates (E) define a zero equipotential region where the beams are crossing at right angles (C). The kinetic energy of the electron beam is controlled by the voltage difference between the cathode (K) and the electrode (E). On both sides of the interaction region, slits (L) collimate the beam and plates (P) play the role of suppressors. A voltage can be applied to these plates in order to establish a potential barrier or a potential well to check the influence of residual gas ions trapped in the electron beam. The electron beam is collected in a Faraday cup (F). Suppressing electrodes (S) provide total beam collection and prevent secondary electrons from interacting with the ion beam. As required by the animated beam method, the electron beam is swept mechanically across the ion beam in a see-saw motion. An optical encoder records the gun position with a precision of 2 μm. The electron gun displacement is produced by means of a step by step motor acting on a rod.

In this kind of experiment, the count rate (N) is related to the cross section (σ) by the general relation

$$N = \sigma L \tag{1}$$

where L is the luminosity. In the present application of the animated beam method, the ionization cross section is related to the measured quantities in the following way (Duponchelle *et al* 1995):

$$\sigma = \frac{H}{n} \frac{v_e v_i q e^2}{\sqrt{v_i^2 + v_e^2}} \sum_{j=1}^{n} \frac{k(j)}{\Delta t(j)\, i_i(j)\, i_e(j)} \tag{2}$$

where $k(j)$ is the number of events produced at position j of the sweeping motion for one passage of the electrons across the ion beam, $\Delta t(j)$ is the time spent at this position, v_e and v_i, e and qe, $i_e(j)$ and $i_i(j)$, are the velocities, charges and currents of the electrons and of the ions, respectively. H is the total vertical displacement of the electron beam and n is the number of steps. The count rate is normalized to average values of time Δt, electron I_e and ion I_i currents.

3. Measurements

The electron and ion currents collected in Faraday cups are frequency converted and recorded according to the electron beam position in a multichannel analyser triggered by the signals showing the position of the encoder. Similar recordings are performed for the amplified detector pulses and for the pulses produced by the internal clock of the computer. The number of events is divided by the time spent at each position and by the corresponding electron and ion currents so that irregularities due to mechanical perturbations do not affect the precision of the cross section measurements.

The detector efficiency has been estimated to be 100% from the pulse height spectrum observation and the total transmission of ions from the collision to the detector has been established.

Table 1. Typical working conditions.

Parameters	Typical value	Systematic error (%)	Statistical error (%)
Kinematic factor	—	0.5	—
Velocity (u, mm s^{-1})	0.48	0.1	—
Electron current (I_e, mA)	5–14	0.5	1.0
Ion current (I_i, nA)			
Kr^{12+}	400	0.5	1.0
Kr^{13+}	450	0.5	1.0
Kr^{14+}	300	0.5	1.0
Kr^{15+}	450	0.5	1.0
Kr^{16+}	300	0.5	1.0
Kr^{17+}	200	0.5	1.0
Kr^{18+}	60	0.5	1.0
Signal (K), Luminosity (L, 10^{19} Hz cm^{-2})			
Kr^{12+}	556/32	1.0	3.1
Kr^{13+}	800/58	1.0	2.0
Kr^{14+}	367/49	1.0	2.1
Kr^{15+}	234/33	1.0	3.0
Kr^{16+}	48/8	1.0	5.9
Kr^{17+}	60/16	1.0	4.5
Kr^{18+}	10/4	1.0	6.3
Cross section (σ, 10^{-19} cm^2)			
Kr^{12+}	17.5	2.6	5.1
Kr^{13+}	13.8	2.6	4.0
Kr^{14+}	7.52	2.6	4.1
Kr^{15+}	7.08	2.6	5.0
Kr^{16+}	5.61	2.6	7.9
Kr^{17+}	3.67	2.6	6.5
Kr^{18+}	2.45	2.6	8.3

The background consists of two distinct contributions. The first one is independent of the particle currents and is caused by the intrinsic background of the detector and by x-rays emitted by the ECR ion source. The second one, which is proportional to the ion current, is due to interactions of primary ions with slits and with residual gas molecules. Reactions producing ions of the same charge and energy as the true signal are charge exchange and stripping. In addition, slow secondary ions may be formed by electron impact on residual gas or at the collector. They can be avoided by suitable polarization of this collector (F) and of the suppressing electrodes (P) and (S). The background from the residual gas is deduced from the flat areas of the spectrum after subtraction of the intrinsic background of the detector.

It is not possible to separate ions having the same charge-to-mass ratio. This situation holds for the $^{84}Kr^{12+}$, $^{84}Kr^{14+}$ and $^{84}Kr^{18+}$ primary ion beam, which is seen to contain $^{14}N^{2+}$, $^{12}C^{2+}$ and $^{14}N^{3+}$ ions, respectively. For these ions, we have performed the measurements by using an ion beam formed of the krypton isotope ^{86}Kr (natural abundance 17.3%). The electron energy is corrected for contact potential (-0.5 eV) and the kinetic energy of ions is taken into account to obtain the absolute collision energy (Duponchelle *et al* 1995). The uncertainty on this energy is ± 0.5 eV. Typical values, corresponding to working conditions of experimental parameters, are given in table 1 together with associated uncertainties.

4. Results and discussion

Absolute cross sections are reported for electron-impact single ionization of Kr^{q+} ($q = 12$–18) in the energy range from below threshold to about 5.5 keV. These results are listed in tables 2–8 and are shown in figures 2–8 for $q = 12$–18, respectively. Error bars represent one standard deviation of the counting statistics.

The structure of the concerned ions is of the form $[Ar]3d^i$ ($i = 0$–6). Due to these complicated structures, threshold energies from spectroscopic data are not available. Theoretical data needed for the discussion of the present results are estimated from the Hartree–Fock structure calculation of Blanke *et al* (1992) and from Sugar and Musgrove (1991). These data are summarized in table 9 together with the data deduced from the present measurement and from the measurement of Oualim *et al* (1995) for $q = 10$ and 11.

It is worth mentioning that no other experimental or theoretical results are available for the present ions, with the exception of the semi-empirical Lotz formula (Lotz 1968). This calculation includes direct ionization from the 3d, 3p, 3s subshells only so that total cross sections are largely underestimated, due to the contribution of indirect processes via 3p, 3s, 2s and 2p excitations followed by autoionization. In the ionization threshold energy range, the contribution of the excitation–autoionization (EA) process is estimated relative to the Lotz semi-empirical formula around the 3p ionization threshold. The range of the probable

Table 2. Total cross section for single ionization of Kr^{12+} by electron impact.

E_e (eV)	σ (10^{-19} cm^2)	$\Delta\sigma$ (10^{-19} cm^2)	E_e (eV)	σ (10^{-19} cm^2)	$\Delta\sigma$ (10^{-19} cm^2)
350	−0.01	0.12	1550	16.64	0.47
380	−0.02	0.17	1600	16.42	0.25
400	0.02	0.20	1610	16.26	0.51
402	0.14	0.19	1620	16.19	0.34
405	0.49	0.18	1625	16.05	0.47
410	1.40	0.22	1630	16.00	0.48
420	2.92	0.25	1635	16.45	0.52
430	4.91	0.26	1640	16.46	0.37
450	6.67	0.27	1650	16.43	0.37
470	8.69	0.32	1680	16.34	0.33
500	10.30	0.33	1700	16.17	0.34
510	10.73	0.33	1750	15.87	0.35
515	10.69	0.36	1800	15.96	0.34
520	11.43	0.39	1900	15.65	0.35
530	12.25	0.32	2000	15.30	0.34
540	13.05	0.30	2100	15.11	0.34
550	13.50	0.35	2200	14.97	0.34
600	14.72	0.31	2300	14.68	0.39
700	16.27	0.43	2400	14.21	0.38
800	16.53	0.40	2500	13.84	0.32
900	17.30	0.44	2800	13.33	0.32
1000	17.56	0.34	3000	12.56	0.29
1100	17.52	0.49	3200	12.24	0.38
1200	17.45	0.49	3500	11.65	0.35
1300	17.23	0.54	4000	11.14	0.38
1400	17.06	0.48	4500	10.43	0.38
1500	16.74	0.50	5000	9.60	0.37

Table 3. Total cross section for single ionization of Kr^{13+} by electron impact.

E_e (eV)	σ (10^{-19} cm^2)	$\Delta\sigma$ (10^{-19} cm^2)	E_e (eV)	σ (10^{-19} cm^2)	$\Delta\sigma$ (10^{-19} cm^2)
400	0.01	0.04	1500	13.11	0.29
420	−0.07	0.08	1550	12.94	0.27
440	−0.01	0.07	1600	12.80	0.27
445	0.07	0.10	1620	12.73	0.28
447	0.37	0.10	1625	12.71	0.29
450	1.16	0.11	1627	12.71	0.27
455	1.93	0.12	1630	12.88	0.27
460	2.62	0.11	1632	12.86	0.27
470	3.65	0.16	1635	12.86	0.20
480	4.69	0.17	1640	12.84	0.29
490	5.55	0.15	1650	12.81	0.27
500	6.41	0.20	1660	12.78	0.20
520	7.39	0.18	1670	12.74	0.20
540	8.55	0.25	1680	12.71	0.27
550	9.04	0.22	1700	12.61	0.18
555	9.08	0.22	1750	12.54	0.21
560	9.17	0.21	1800	12.38	0.25
565	9.43	0.23	1900	12.21	0.26
570	9.66	0.15	2000	11.98	0.25
580	10.11	0.23	2100	11.84	0.24
600	10.50	0.24	2150	11.67	0.25
650	11.32	0.25	2200	11.52	0.24
700	12.21	0.26	2300	11.36	0.26
800	13.34	0.30	2400	10.95	0.25
900	13.46	0.28	2600	10.60	0.22
900	13.48	0.28	2800	10.38	0.24
1000	13.73	0.23	3000	10.05	0.23
1100	13.60	0.28	3500	9.23	0.25
1200	13.52	0.29	4000	8.70	0.24
1300	13.34	0.22	4500	8.27	0.24
1400	13.31	0.22	5000	7.74	0.26

autoionizing states was estimated for each ion by assuming that the ionization potential of an excited state is given by

$$I(n) = \frac{A}{n^2} \tag{3}$$

where n is the principal quantum number and the constant A is determined by using the known ground state threshold (table 9).

The relative importance of 2s–nl and 2p–nl ($n \geqslant 3$) excitation–autoionization processes is estimated roughly at the lowest threshold ($nl = 3$d).

For Kr^{14+}, Kr^{16+} and Kr^{18+} important signals are observed below the ground state ionization threshold indicating the presence of metastable states in the primary ion beam. For each of these ions, the metastable state is identified from the comparison of the experimental value of the ionization threshold with the calculated data. The observed metastable state belongs to the ground configuration for Kr^{14+} and Kr^{16+}. For Kr^{18+}, which belongs to the argon isoelectronic sequence, the lowest excited configuration is observed. Due to the large number of states existing in the concerned configurations, it is not possible to precisely determine which states contribute to the observed signal.

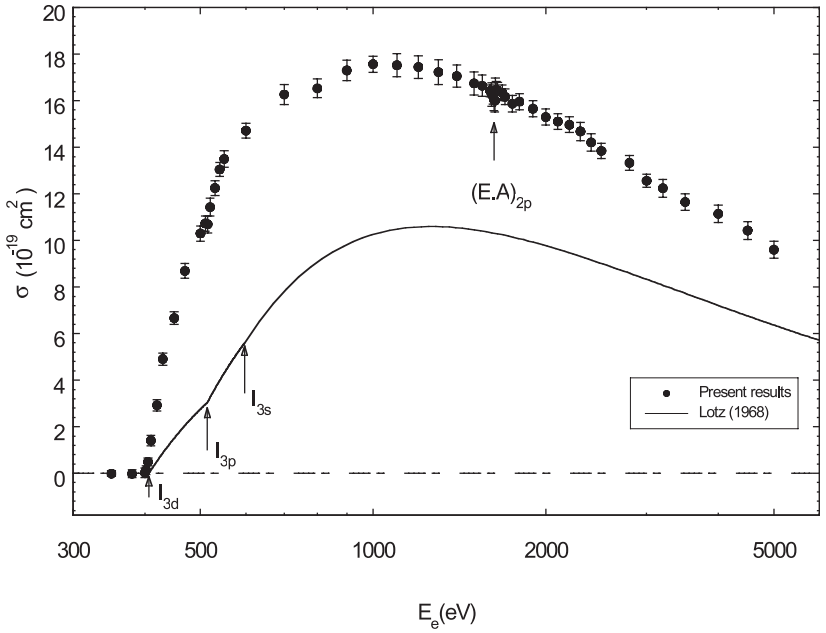

Figure 2. Absolute cross section for electron-impact single ionization of Kr^{12+}. Dots (●) are the present experimental results. I_{3d}, I_{3p} and I_{3s} are the ionization thresholds for the 3d, 3p and 3s ground configuration subshells, respectively. $(EA)_{2p}$ indicates the 2p–3d excitation threshold. The full curve represents the semi-empirical Lotz formula for the ground state.

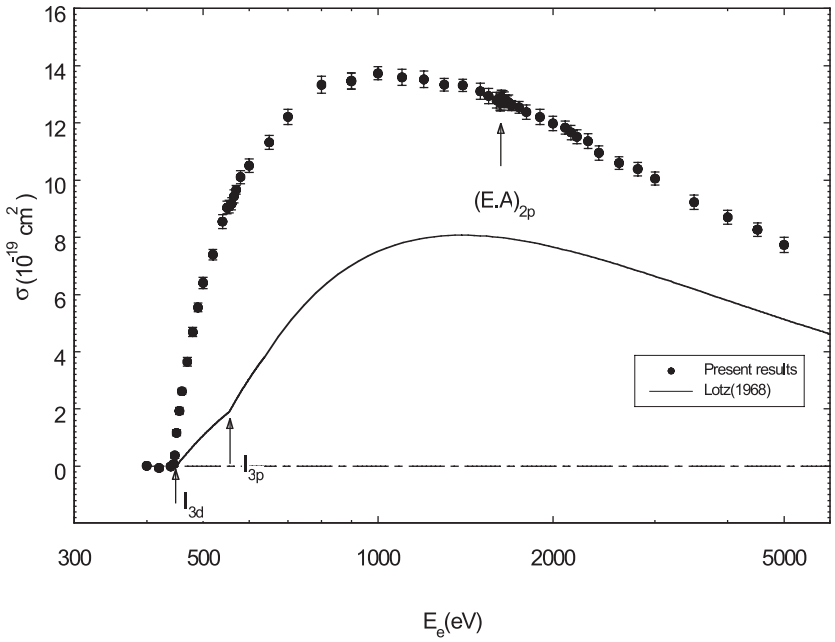

Figure 3. Absolute cross section for electron-impact single ionization of Kr^{13+}. Symbols are identical to figure 2.

Table 4. Total cross section for single ionization of Kr^{14+} by electron impact.

E_e (eV)	σ (10^{-19} cm^2)	$\Delta\sigma$ (10^{-19} cm^2)	E_e (eV)	σ (10^{-19} cm^2)	$\Delta\sigma$ (10^{-19} cm^2)
460	0.0001	0.0465	1000	7.93	0.13
470	0.03	0.03	1100	7.97	0.13
475	0.04	0.04	1200	7.79	0.12
480	0.07	0.04	1300	7.72	0.12
482	0.18	0.04	1400	7.57	0.14
485	0.27	0.05	1500	7.54	0.08
487	0.42	0.03	1550	7.52	0.12
490	0.70	0.03	1600	7.46	0.10
495	1.00	0.06	1620	7.30	0.15
500	1.35	0.05	1630	7.36	0.17
510	2.06	0.07	1640	7.42	0.17
520	2.61	0.08	1650	7.56	0.16
530	3.22	0.07	1660	7.52	0.17
540	3.55	0.08	1670	7.51	0.18
550	4.14	0.06	1680	7.44	0.17
565	4.57	0.10	1700	7.32	0.09
570	4.63	0.08	1750	7.25	0.10
575	4.72	0.11	1800	7.14	0.11
580	4.78	0.08	1850	7.04	0.15
585	4.94	0.10	1900	7.02	0.15
590	5.21	0.11	2000	6.79	0.17
600	5.43	0.12	2500	6.53	0.17
650	6.10	0.13	3000	5.81	0.16
700	6.59	0.01	3500	5.48	0.16
800	7.43	0.17	4000	5.15	0.18
900	7.69	0.16	5000	4.34	0.20

4.1. Kr^{12+}

The lowest ionization threshold is clearly observed around 401 eV (see table 9). This is in good agreement with the ground state ionization threshold, deduced from single- and double-ionization cross section measurements for Kr^{11+} (Oualim *et al* 1995). No theoretical or experimental result can be compared with the present experimental data, except the semi-empirical Lotz formula (Lotz 1968). Taking into account the 3s, 3p and 3d ground state contribution, the cross section prediction underestimates the measured absolute cross section by some 50% around the maximum. In the threshold energy region, this difference is due mainly to the contribution of excitation of 3s and 3p electrons to highly excited states 3s–*nl* ($n \geqslant 6$) and 3p–*nl* ($n \geqslant 7$) which increase the total cross section by about 71%. A similar effect was discussed for the isoelectronic Ni^{4+} (Stenke *et al* 1995). In that case, the average configuration distorted-wave calculation of Pindzola *et al* (1991) was found to be in good agreement with the experimental data of Stenke *et al* (1995).

The 2p–3d excitation–autoionization contribution threshold is observed at 1632 eV, in satisfactory agreement with the prediction of Blanke *et al* (1992). This contribution is found to be very weak.

Table 5. Total cross section for single ionization of Kr^{15+} by electron impact.

E_e (eV)	σ (10^{-19} cm^2)	$\Delta\sigma$ (10^{-19} cm^2)	E_e (eV)	σ (10^{-19} cm^2)	$\Delta\sigma$ (10^{-19} cm^2)
500	−0.002	0.042	1300	7.17	0.18
530	−0.003	0.087	1400	7.06	0.17
535	0.01	0.05	1500	7.09	0.09
540	0.02	0.08	1550	7.05	0.16
545	0.03	0.11	1600	7.09	0.10
548	0.16	0.11	1620	7.00	0.15
550	0.41	0.14	1630	7.03	0.23
560	0.85	0.08	1640	7.09	0.19
570	1.45	0.17	1645	7.21	0.23
580	2.23	0.14	1650	7.40	0.12
600	2.83	0.10	1660	7.41	0.22
620	3.47	0.18	1670	7.41	0.20
640	4.03	0.21	1680	7.34	0.17
645	4.01	0.19	1700	7.37	0.24
650	4.09	0.19	1750	7.29	0.10
660	4.41	0.17	1800	7.22	0.10
680	4.74	0.17	1850	7.22	0.13
700	5.13	0.16	1900	7.15	0.10
750	5.65	0.13	1950	7.08	0.13
800	5.92	0.13	2000	6.96	0.09
850	6.28	0.17	2200	6.83	0.18
900	6.56	0.17	2500	6.56	0.20
950	6.81	0.16	3000	6.19	0.14
1000	6.92	0.17	3500	5.90	0.22
1100	7.01	0.16	4000	5.61	0.20
1200	6.97	0.11	4500	5.31	0.17

4.2. Kr^{13+}

The first threshold is observed around 446 eV, in good agreement with the calculated ground state ionization threshold, 449.6 eV. The 3s–*nl* ($n \geqslant 7$) and 3p–*nl* ($n \geqslant 6$) EA processes contribute to the total cross section for some 79%. This contribution was also observed for the Ni^{5+} isoelectronic ion where the agreement between experimental and theoretical data was excellent (Stenke *et al* 1995).

The enhancement of the cross section due to the 2s–3d and 2p–3d EA transitions is observed at 1628 eV, and is about 1.4% of the total cross section.

4.3. Kr^{14+}

The first threshold is clearly observed around 478 eV, which is 13.8 eV below the theoretical ground state threshold (Sugar and Musgrove 1991). This energy difference indicates that metastable states are present in the primary ion beam.

The indirect contribution of the 3s and 3p excitation followed by autoionization is about 78% of the total cross section. The 3p–*nl* and 3s–*nl* transitions are autoionizing for $n \geqslant 8$ and $n \geqslant 6$, respectively.

For the titanium-like ion Ni^{6+}, these transitions are autoionizing for $n \geqslant 4$ and $n \geqslant 3$ (Pindzola *et al* 1991). Experimental data of Wang *et al* (1988) were compared with distorted-wave calculations for direct ionization only. It was shown that these indirect contributions are

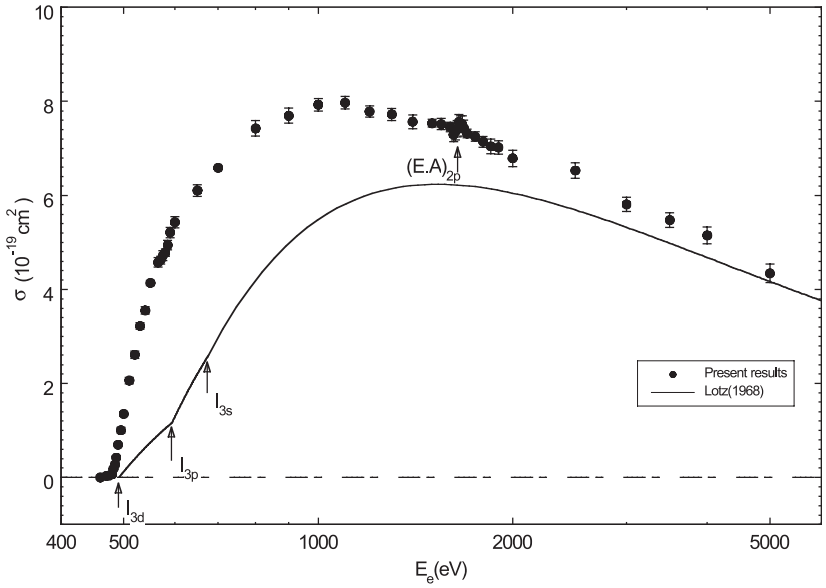

Figure 4. Absolute cross section for electron-impact single ionization of Kr^{14+}. Symbols are identical to figure 2.

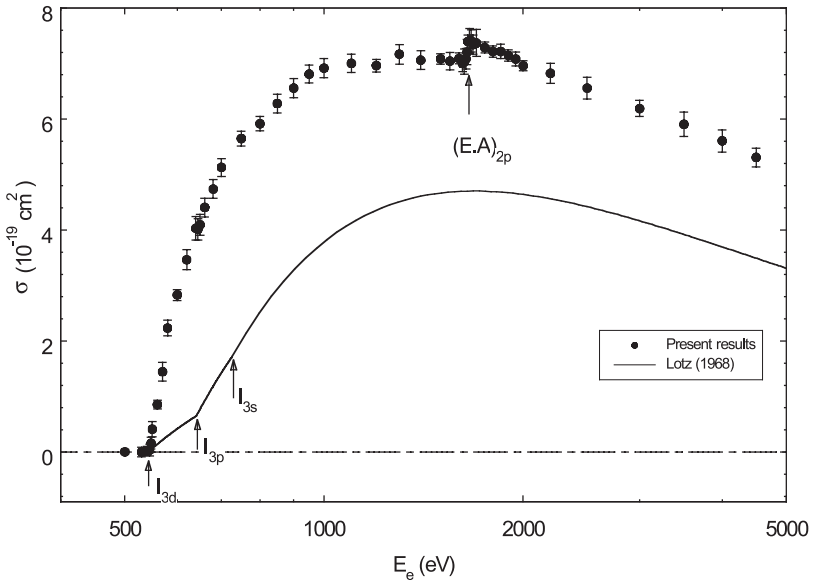

Figure 5. Absolute cross section for electron-impact single ionization of Kr^{15+}. Symbols are identical to figure 2.

for about 25% of the measured peak total ionization cross section.

Around 1645 eV, a weak contribution is observed due to the excitation–autoionization process involving the 2p–3d transition predicted at 1640 eV. This contribution is about 3.2% of the total measured cross section.

Table 6. Total cross section for single ionization of Kr^{16+} by electron impact.

E_e (eV)	σ (10^{-19} cm^2)	$\Delta\sigma$ (10^{-19} cm^2)	E_e (eV)	σ (10^{-19} cm^2)	$\Delta\sigma$ (10^{-19} cm^2)
500	0.004	0.14	1200	5.34	0.11
550	−0.02	0.20	1300	5.43	0.21
580	0.04	0.04	1400	5.65	0.23
585	0.02	0.23	1500	5.59	0.11
590	0.08	0.21	1580	5.46	0.30
595	0.14	0.27	1600	5.50	0.11
600	0.15	0.14	1605	5.38	0.34
605	0.45	0.21	1610	5.42	0.31
610	0.67	0.30	1615	5.52	0.34
615	0.73	0.29	1640	5.50	0.11
620	0.96	0.16	1650	5.46	0.15
630	1.41	0.27	1660	5.92	0.16
640	1.68	0.22	1700	5.98	0.15
650	1.85	0.17	1750	6.05	0.19
670	2.14	0.36	1800	6.09	0.36
700	2.27	0.18	1850	6.04	0.42
720	2.67	0.19	1900	6.04	0.22
750	2.88	0.22	2000	6.00	0.16
800	3.26	0.11	2200	5.88	0.23
850	3.72	0.17	2500	5.42	0.33
900	4.25	0.24	3000	4.65	0.33
1000	4.64	0.15	3500	4.16	0.36
1100	5.24	0.17	4000	3.75	0.27

4.4. Kr^{15+}

The measurement shows a good agreement of the observed threshold (542 eV) with the calculated ionization energy of the 3d ground state. The Lotz formula prediction underestimated the total cross section by about 83%. This difference is due to 3p–*nl* and 3s–*nl* transitions, which may lead to autoionization for $n \geqslant 8$ and $n \geqslant 6$, respectively.

In the Ni^{7+} case, experimental data are compared with distorted-wave calculations for direct ionization (Wang *et al* 1988). It is seen that these indirect contributions are about 35% of the measured peak total ionization cross section. A similar calculation (Pindzola *et al* 1991), including 3p–*nl* ($n \geqslant 4$) and 3s–*nl* ($n \geqslant 4$) excitations and direct ionization of 3s, 3p and 3d of the Ni^{7+}, is found to be in excellent agreement with the measurement. For Fe^{5+}, the excitation–autoionization contribution near the threshold enhances the direct ionization by more than 50% (Pindzola *et al* 1986).

At 1645 eV, the additional contribution corresponding to the 2p–*nl* and 2s–*nl* transitions increases the total cross section by about 5.4%.

4.5. Kr^{16+}

The first threshold is observed around 585 eV, which is 8 eV below the ground state theoretical threshold (Blanke *et al* 1992). This is the signature of the presence of metastable states in the primary ion beam.

Three ions have been previously analysed in the calcium isoelectronic sequence. Ni^{8+} ions were found to be formed in the $3p^6 3d4s$ metastable configuration with an estimated population

Table 7. Total cross section for single ionization of Kr^{17+} by electron impact.

E_e (eV)	σ (10^{-19} cm^2)	$\Delta\sigma$ (10^{-19} cm^2)	E_e (eV)	σ (10^{-19} cm^2)	$\Delta\sigma$ (10^{-19} cm^2)
600	0.03	0.06	1600	3.63	0.12
620	0.00	0.13	1650	3.60	0.12
630	0.00	0.05	1655	3.82	0.16
640	0.02	0.12	1660	4.05	0.18
650	0.13	0.12	1670	4.11	0.13
660	0.27	0.12	1680	4.00	0.10
680	0.40	0.11	1700	4.07	0.10
700	0.60	0.12	1750	4.14	0.14
730	0.83	0.15	1800	4.16	0.17
740	1.04	0.12	1850	4.16	0.15
750	1.40	0.09	1900	4.15	0.11
770	1.78	0.11	1950	4.09	0.12
800	2.19	0.10	2000	4.06	0.15
850	2.51	0.08	2100	4.04	0.24
900	2.84	0.09	2200	4.01	0.15
1000	3.09	0.07	2400	3.90	0.24
1100	3.17	0.10	2700	3.73	0.21
1200	3.29	0.12	3000	3.54	0.10
1300	3.42	0.12	3500	3.25	0.15
1400	3.50	0.14	4000	2.88	0.24
1500	3.58	0.14	4500	2.62	0.21

Table 8. Total cross section for single ionization of Kr^{18+} by electron impact.

E_e (eV)	σ (10^{-19} cm^2)	$\Delta\sigma$ (10^{-19} cm^2)	E_e (eV)	σ (10^{-19} cm^2)	$\Delta\sigma$ (10^{-19} cm^2)
600	0.002	0.014	1500	2.45	0.15
650	−0.007	0.039	1550	2.45	0.15
700	0.003	0.045	1580	2.43	0.18
720	0.05	0.01	1585	2.36	0.19
740	0.07	0.05	1587	2.57	0.17
750	0.15	0.09	1590	2.87	0.19
760	0.19	0.10	1595	3.10	0.18
780	0.30	0.14	1600	3.01	0.13
800	0.41	0.14	1700	3.02	0.21
825	0.50	0.13	1800	3.08	0.19
850	0.63	0.15	1900	3.09	0.13
880	0.84	0.17	2000	3.02	0.13
900	1.02	0.17	2200	3.02	0.13
950	1.33	0.15	2500	2.82	0.12
1000	1.58	0.10	2750	2.63	0.18
1050	1.67	0.20	3000	2.45	0.17
1100	1.97	0.13	3500	2.30	0.21
1200	2.17	0.11	4000	2.14	0.20
1300	2.30	0.10	4500	2.05	0.27
1400	2.40	0.10	5000	1.97	0.31
1440	2.43	0.19			

Table 9. Observed and calculated reaction thresholds for the states and transitions involved in this work. [Ar], $1s^2 2s^2 2p^6 3s^2 3p^6$; [Ar*], $1s^2 2s^2 2p^6 3s^2 3p^5 3d$; (m), metastable state; (g), ground state; n, principal quantum number for $3p \rightarrow nl$ and $3s \rightarrow nl$ autoionizing transitions; I_{th}, $(EA)^{th}_{nl}$, theoretical thresholds (Blanke *et al* 1992); EA, excitation–autoionization; I_{obs}, lowest ionization threshold observed in this work.

Ions	Ground state	Observed state	I_{obs} (eV)	I_{th} (eV)	n $3p \rightarrow nl$	n $3s \rightarrow nl$	$(EA)^{obs}_{2p}$ (eV)	$(EA)^{th}_{2p}$ (eV)	$(EA)^{th}_{2s}$ (eV)
$^{86}Kr^{18+}$	$[Ar]^1S$	[Ar*] (m)	703 ± 10	700.2 (m)	$n \geqslant 9$	$n \geqslant 7$	1588 ± 2	1599.0 (m)	1848.6 (m)
$^{84}Kr^{17+}$	$[Ar]3d^1\ ^2D$	^2D (g)	637 ± 5	641.3	$n \geqslant 9$	$n \geqslant 6$	1655 ± 5	1671.3	1921.9
$^{84}Kr^{16+}$	$[Ar]3d^2\ ^3F$	(m)	585 ± 5	593.0 (g)	$n \geqslant 9$	$n \geqslant 6$	1650 ± 5	1661.0 (g)	1912 (g)
$^{84}Kr^{15+}$	$[Ar]3d^3\ ^4F$	^4F (g)	542 ± 3	542.8	$n \geqslant 8$	$n \geqslant 6$	1645 ± 5	1650.0	1900
$^{86}Kr^{14+}$	$[Ar]3d^4\ ^5D$	(m)	478 ± 3	491.8 (g)[b]	$n \geqslant 8$	$n \geqslant 6$	1645 ± 5	1640.0 (g)	1891 (g)
$^{84}Kr^{13+}$	$[Ar]3d^5\ ^6S$	^6S (g)	446 ± 2	449.6	$n \geqslant 7$	$n \geqslant 6$	1628 ± 2	1630.0	1874
$^{86}Kr^{12+}$	$[Ar]3d^6\ ^5D$	^5D (g)	401 ± 1	400 ± 2[a]	$n \geqslant 7$	$n \geqslant 6$	1632 ± 3	1628.0 (g)	1866 (g)
$^{84}Kr^{11+}$	$[Ar]3d^7\ ^4F$	^4F (g)	360 ± 1[a]	360.0	$n \geqslant 7$	$n \geqslant 6$	−1621.5	1858	
$^{84}Kr^{10+}$	$[Ar]3d^8\ ^3F$	^3F (g)	314 ± 1[a]	314.0	$n \geqslant 6$	$n \geqslant 5$	−1615.3	1852	

[a] Oualim *et al* (1995).
[b] Sugar and Musgrove (1991).

of about 10% (Wang *et al* 1988). No metastable contribution was observed for Ti^{2+} (Diserens *et al* 1988) and for Fe^{6+} (Pindzola *et al* 1986).

Beyond the first threshold, the Lotz calculation underestimates the measured cross section by about 85%. This indicates clearly that an important excitation–autoionization plays a significant role. 3p–*nl* and 3s–*nl* transitions lead to autoionization for $n \geqslant 9$ and $n \geqslant 6$, respectively.

In this isoelectronic sequence ion, experimental data are compared with distorted-wave calculations for direct ionization for Ni^{8+} (Wang *et al* 1988) and for Fe^{6+} (Gregory *et al* 1986). The comparison exhibits an indirect contribution of 35% and 30% of the measured peak total ionization cross section, respectively. Moreover, the same calculation including 3p–*nl* ($n \geqslant 5$) and 3s–*nl* excitations and direct ionization of 3s, 3p and 3d of the Ni^{8+} is in good agreement with the measurement (Pindzola *et al* 1991).

In addition, around 1655 eV the threshold excitation–autoionization of 2p is clearly observed. This contribution increases the total cross section by some 10%.

4.6. Kr^{17+}

The measured cross section is well below the zero threshold observed at 637 eV. This value is in good agreement with the 3d ground state threshold calculated at 641 eV. No metastables were found in a primary ion beam. The change of slope observed around 745 eV, indicates that direct ionization from the 3p shell plays a role for this ion. At the 3p ionization threshold, the Lotz formula underestimates the measured cross section by about 86%. This discrepancy corresponds to the contribution of 3s–*nl* and 3p–*nl* transitions, which are autoionizing for $n \geqslant 6$ and $n \geqslant 9$, respectively.

For the potassium-like Ti^{3+} ion, the large enhancement in the threshold cross section was found to be due mainly to 3p–3d excitation–autoionization (Burke *et al* 1984, Gorczyca *et al* 1994b). In the Ni^{9+} case, a ACDW calculation, including 3s–*nl* and 3p–*nl* ($n \geqslant 3$) excitation–autoionization, has shown that the largest excitation contribution is due to the 3p–5f transition (Pindzola 1991). For Sc^{2+}, a similar calculation has shown that the cross section for excitation of the 3p–3d transition is an order of magnitude larger than that of the 3p–4*l* one (Pindzola

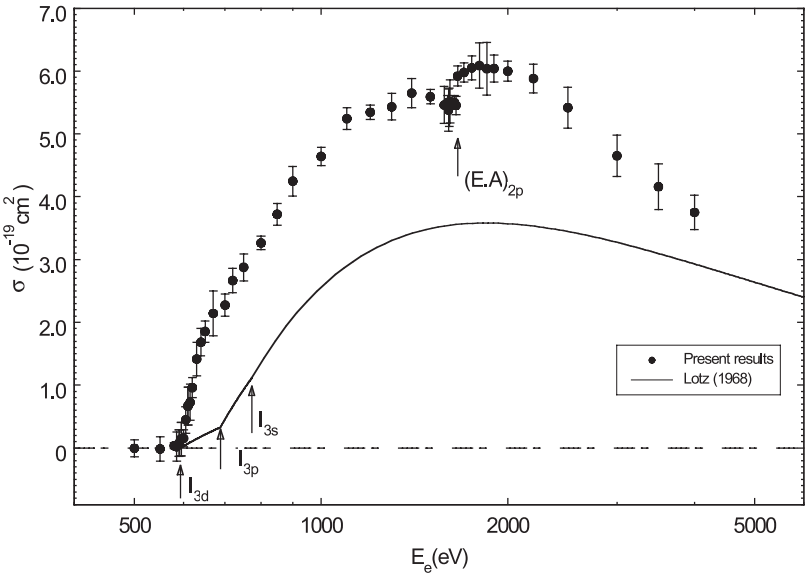

Figure 6. Absolute cross section for electron-impact single ionization of Kr^{16+}. Symbols are identical to figure 2.

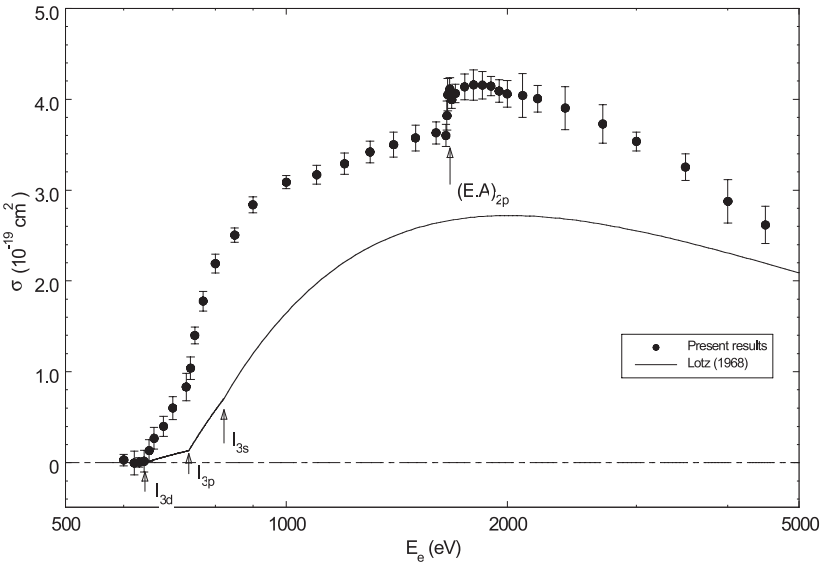

Figure 7. Absolute cross section for electron-impact single ionization of Kr^{17+}. Symbols are identical to figure 2.

et al 1994). EA involving the 2p–3d transition is observed around 1655 eV. This contribution is about 13% of the total cross section.

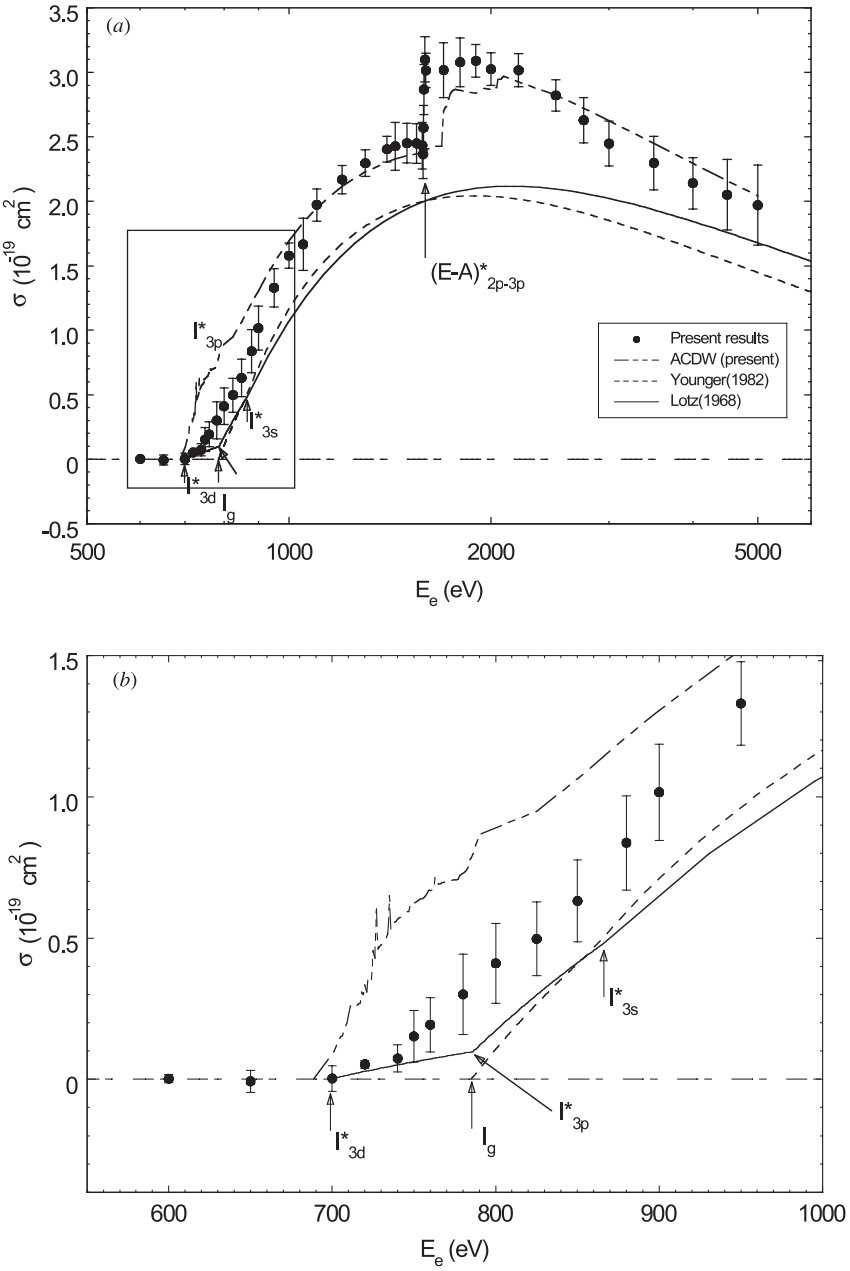

Figure 8. Absolute cross section for electron-impact single ionization of Kr^{18+}. Dots (●) are present experimental results. I_g is the ionization threshold for the ground state. I^*_{3d}, I^*_{3p} and I^*_{3s} are the 3d, 3p and 3s subshell ionization thresholds for the metastable state ($1s^2 2s^2 2p^6 3s^2 3p^5 3d(^3P)$), respectively. $(EA)^*_{2p}$ indicates the 2p–3p excitation threshold for the metastable state. The full curve is the semi-empirical Lotz formula for the metastable state only. The broken curve is the distorted-wave Coulomb Born calculation of Younger (1982) for the ground state only. The chain curve is the present ACDW calculation for the metastable state only.

4.7. Kr^{18+}

Kr^{18+} belongs to the argon isoelectronic sequence. The first threshold is observed around 703 eV, which is 83 eV below the ground state ionization threshold (Blanke *et al* 1992, Shirai *et al* 1995). It is clear that the primary ion beam contains a dominant population corresponding to the metastable excited configuration ($1s^2 2s^2 2p^6 3s^2 3p^5 3d$) for which the lowest ionization threshold is 700.2 eV (Blanke *et al* 1992).

The result is compared (figure 8) to the calculation of Younger (1982) obtained in the distorted-wave Born approximation for direct ionization of the 3s and 3p subshells for the ground state. For the metastable configuration, the Lotz semi-empirical formula for direct ionization of the 3s, 3p and 3d subshells is shown together with the results of a ACDW calculation. The same theoretical method was applied previously for Kr^{10+} and Kr^{11+} (Teng *et al* 2000). The detailed description and discussion of the calculation will be published later.

In the threshold energy region, we note that the disagreement between the experimental results and the prediction of the Lotz formula is much smaller than observed for the lower charge states. This indicates that the 3p–*nl* and 3s–*nl* EA processes play a lower role here. These transitions are autoionizing for $n \geqslant 9$ and $n \geqslant 7$, respectively. In the argon isoelectronic sequence, this indirect contribution was discussed preciously for Ti^{4+} (Hartenfeller *et al* 1998), Cr^{6+} (Satake *et al* 1989) and Ni^{10+} (Pindzola *et al* 1991, Cherkani-Hassani *et al* 2000). For Ti^{4+}, the $3p^5 3d$ excited configuration contribution was clearly seen to dominate over the ground state contribution. The 3p–*nl* and the 3s–*nl* transitions, which lead to autoionization for $n \geqslant 5$ and $n \geqslant 3$, respectively, increase the total cross section by about 24%. In the Cr^{6+}case, the calculation for excited ions still significantly underestimates the measured cross section. This discrepancy was attributed to excitation–autoionization from the 3s subshell of the metastable configuration. For Ni^{10+}, the metastable population of the $3p^5 3d$ excited configuration is estimated to be 84%. The difference between the total and direct ionization cross sections for the excited configuration is due solely to the 3n–*nl* transitions. Including this indirect process, the Pindzola calculation still underestimated the measured cross section by about 20% (Cherkani-Hassani *et al* 2000).

The cross section enhancement observed for the Kr^{18+} ion above 1598 eV is attributed to 2n–*nl* EA from the ground and/or from the metastable configuration. The largest contribution is due to the 2p–3p transition. This indirect process increases the cross section by about 25%.

The calculation is performed in the ACDW approximation in the case where the ion is formed in the metastable excited state. Both direct ionization and EA processes are included. The direct ionization cross section is calculated for the ejection of electrons belonging to the 3s, 3p and 3d subshells. EA contributions are calculated for the following transitions: 3p–*nl* ($n = 8$–10), 3s–*nl* ($n = 6$–8), 2p–3p, 2p–3d, 2p–4*l* ($l = 0$–3), 2s–3p, 2s–3d, 2s–4*l* ($l = 0$–3). In the threshold energy region, this calculation clearly overestimates the role of the 3p–*nl* and 3s–*nl* autoionizing transitions. The agreement between theory and experiment is very good above 1000 eV with the exception of the contribution of the 2p–3p transition which is not reproduced by the calculation. Further developments of the calculation should improve the agreement between theory and experiment.

5. Summary and conclusion

The present absolute cross sections are shown in figure 9 for all the charge states concerned. The figure shows clearly the increasing role of excitation to autoionizing states via the 2p–3*l* transitions. One generally expects that the ionization cross section will reduce as the ion charge increases. In the present study, the cross section for $q = 14$ exceeds the one for $q = 15$

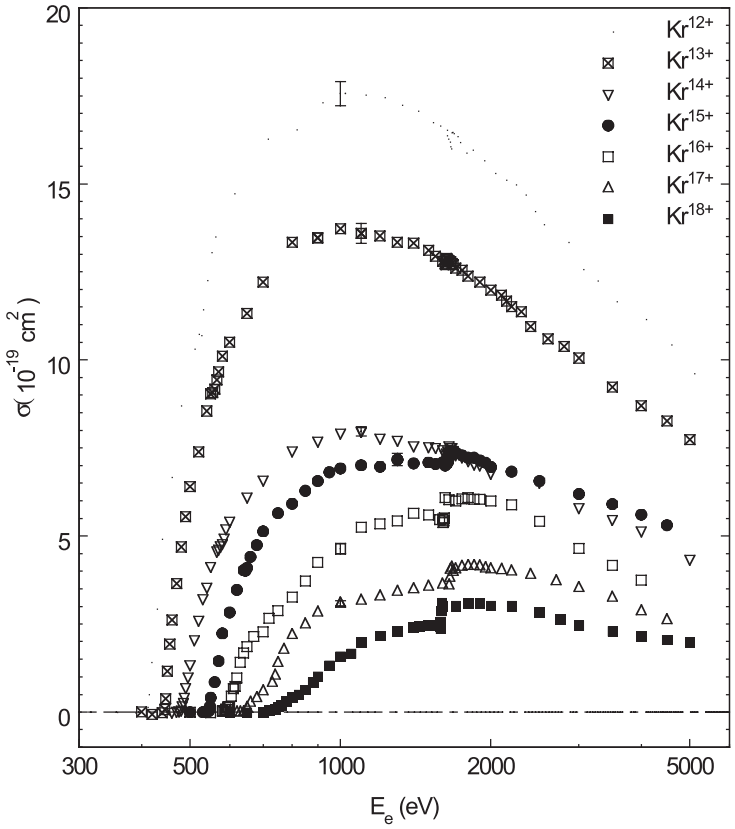

Figure 9. Absolute cross sections for electron-impact single ionization of multicharged Kr^{q+} ($q = 12$–18) ions.

above the 2p–3p excitation–autoionization threshold. Detailed calculations should give an explanation of this effect.

The presence of ions formed in metastable states belonging to the ground configuration is observed for Kr^{14+} and Kr^{16+} but for Kr^{18+}, the observed metastable state belongs to the lowest excited configuration. The important signals observed below the ground state ionization threshold indicate that the corresponding metastable state population is probably dominant for all the concerned ions. It is not possible to estimate the metastable population in the present experiment.

The comparison of experimental results with the prediction of the semi-empirical Lotz formula shows the dominant role of the excitation–autoionization processes in the low-energy range. The ACDW calculation performed for Kr^{18+} in the metastable state only will be improved in order to explain most of the experimental observations. It will also be extended to charge states 12–17.

It is interesting to relate the absence of any spectroscopic data corresponding to the present studied ions. The one and only source of information being the calculation of Blanke *et al* (1992), the present energy data (table 9) are, up to now, the first experimentally determined ionization and excitation thresholds for these ionic species.

Acknowledgments

The authors acknowledge B Fricke of University of Kassel (Germany) for providing us with their ion energy database.

References

Bannister M E, Guo X Q and Kajima T M 1994 *Phys. Rev.* A **49** 4676
Bannister M E, Mueller D W, Wang L J, Pindzola M S, Griffin D C and Gregory D C 1988 *Phys. Rev.* A **38** 38
Barué C, Biri S, Cherkani-Hassani S, Gealens M, Loiselet M and Ryckewaerst G 1998 *Rev. Sci. Instrum.* **69** 764
Blanke J H, Fricke B and Finkbener M 1992 *Database Plasmarelevante Atomare Daten* University of Kassel, Germany
Burke P G, Fon W C and Kingston A E 1984 *J. Phys. B: At. Mol. Phys.* **17** L733
Cherkani-Hassani S, Khouilid M and Defrance P 2000 *10th Int. Conf. on the Physics of Highly Charged Ions (Berkeley, CA)*
Defrance P 1995 *Nucl. Fusion Suppl.* **6** 43
Defrance P, Brouillard F, Claeys W and Van Wassenhove G 1981 *J. Phys. B: At. Mol. Phys.* **14** 103
Defrance P, Duponchelle M and Moores D L 1995 *Atomic and Molecular Processes in Fusion Edge Plasmas* ed R K Janev (New York) p 153
Diserens M J, Smith A C H and Harrison M F A 1988 *J. Phys. B: At. Mol. Opt. Phys.* **21** 2129
Duponchelle M, Zhang M, Oualim E M, Bélenger C and Defrance P 1995 *Nucl. Instrum. Methods* A **364** 159
Gorczyca T W, Pindzola M S, Badnell N R and Griffin D C 1994a *Phys. Rev.* A **49** 4682
Gorczyca T W, Pindzola M S, Griffin D C and Badnell N R 1994b *J. Phys. B: At. Mol. Opt. Phys.* **27** 2399
Gregory D C 1985 *Nucl. Instrum. Methods* B **10/11** 87
Gregory D C and Bannister M E 1994 *Report ORNL/TM-12729* Oakridge National Laboratory, TN, USA
Gregory D C, Ditner P F and Crandall 1983 *Phys. Rev.* A **24** 724
Gregory D C, Meyer F W, Müller A and Defrance P 1986 *Phys. Rev.* A **34** 3657
Hartenfeller U, Aichele K, Hathiramani D, Hofmann G, Schäfer V, Steidl M, Stenke M, Salzborn E and Pindzola M S 1998 *J. Phys. B: At. Mol. Opt. Phys.* **31** 2999
Janev R K 1993 Summary report of the IAEA Technical Committee Meeting on atomic and molecular fusion reactor technology *Report* INDC(NDS-277) (Vienna: International Atomic Energy Agency)
Lotz W 1968 *Z. Phys.* **216** 241
Man K F, Smith A C H and Harrison M F A 1987 *J. Phys. B: At. Mol. Phys.* **20** 5865
——1993 *J. Phys. B: At. Mol. Opt. Phys.* **26** 1365
Oualim E M, Duponchelle M and Defrance P 1995 *Nucl. Instrum. Methods* B **98** 150
Pindzola M S, Gorczyca T W, Griffin D C, Badnell N R, Müller A and Dunn G H 1994 *Phys. Rev.* A **49** 933
Pindzola M S, Griffin D C and Bottcher C 1986 *Phys. Rev.* A **34** 3668
Pindzola M S, Griffin D C, Bottcher C, Buie M J and Gregory D C 1991 *Phys. Scr.* T **37** 35
Sataka M, Ohtani S, Swenson D and Gregory D C 1989 *Phys. Rev.* A **39** 2397
Shirai T, Okazaki K and Sugar J 1995 J. *Phys. Chem. Ref. Data* **24** 1577
Stenke M, Hathiramini D, Hofmann G, Shevelko V P, Steidl M, Völpel R and Salzborn E 1995 *Nucl. Instrum. Methods* B **98** 138
Sugar J and Musgrove A 1991 *J. Phys. Chem. Ref. Data* **20** 859
Teng H, Defrance P, Chen C and Wang Y 2000 *J. Phys. B: At. Mol. Opt. Phys.* **33** 463
Tinschert K, Müller A, Hofmann G, Achenbach Ch, Becker R and Salzborn E 1987 *J. Phys. B: At. Mol. Phys.* **20** 1121
Wang L J, Rinn K and Gregory D C 1988 *J. Phys. B: At. Mol. Opt. Phys.* **21** 2117
Younger S M 1982 *Phys. Rev.* A **26** 3177